Analysis of Coil Coupling in the Near-field Far-field Hybrid Region

Erda Wen, Daniel F. Sievenpiper, Fellow, IEEE, and Patrick P. Mercier, Senior Member, IEEE

Abstract—In this letter, we quantitatively analyze the mechanism of two coils working in the near-field/far-field hybrid zone. In particular, we propose to separate the coupling in terms of static and radiative, rather than the ambiguous near or far field. The results of our impedance matrix model show that the domination of the two mechanisms depends on both the antenna geometry and the antenna arrangement. We demonstrate how one may take advantage of the hybrid coupling mechanism to acquire maximized gain and to broaden the channel bandwidth.

Index Terms—near-field communication, electromagnetic coupling

I. INTRODUCTION

EAR-field magnetic systems have drawn considerable attention in recent years to enable efficient wireless communication or power transfer applications within short distances such as wireless power transfer (WPT) [1] and nearfield human body communication (HBC) [2], [3]. These approaches are reported to be more efficient and more robust over conventional far-field RF radio channels when in proximity to lossy mediums like the human body, since the near-field component suffers much less from the large path loss and scattering in comparison with the radiative energy flux [4].

Despite the fact that near-field and far-field communication hold very different characteristics, the boundary between them is not strictly defined. This has been mostly acceptable for earlier near-field coupling studies since they generally adopt such low frequencies and short ranges that a quasi-static state can be reasonably assumed and the system can be modeled with static field calculation [5], or even more simply, circuit models [6], [7]. However, some recent research tend to adopt much higher frequencies at longer distances [2], where the ambiguity in the near-field definition starts to cause problems for modeling the transmission mechanism and for designing a legitimate measurement platform: the E-field/H-field dominant quasi-static model is no longer valid, as Fig. 1 shows, under which circumstance, pitfalls like poor ground isolation in measurement may lead to deceptively optimistic results as noted in [3], [8].

It is worth noting that the widely accepted near-field boundary definitions, such as $2D^2/\lambda$, $0.62\sqrt{D^3/\lambda}$, or $\lambda/2\pi$, as very rough definitions, do not help when it comes to modeling systems working at around that distance - the so-called hybrid near-field/far-field region. In this paper, we examine the

The authors are with the Electrical and Computer Engineering Department, University of California San Diego, La Jolla, CA 92093-0021 USA (e-mail: ewen@ucsd.edu). This work was supported in part by the National Science Foundation under Grant 1751293.

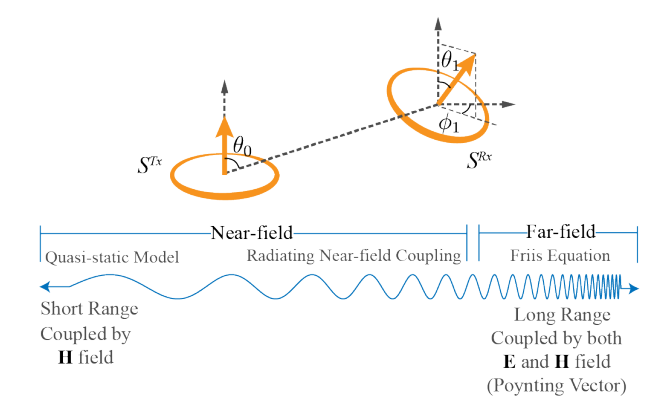


Fig. 1. Mechanism of coupling between coils at various distances and frequencies, and the proper models to analyze the system.

transmission between two coils with coupling mode methods and, more importantly, we distinguish the static inductive part from the radiative part to illustrate what happens in the near-field/far-field hybrid region. With this model, we quantitatively demonstrate the advantages as well as limitations of a channel link with a higher static coupling, in terms of efficiency and bandwidth.

II. STATIC AND RADIATIVE COUPLING BETWEEN COILS

Before stepping into the analysis of whether coupling between Tx and Rx is static or radiative, a rigorous definition of those two terms is needed. Here we define static coupling as the energy transfer through a pure imaginary Poynting vector, like a transformer coil does, while on the other hand, radiative coupling refers to the energy transfer through a real Poynting vector, through which far-field antennas can communicate with each other.

For two coils working in the hybrid region, we may model the system with a Z matrix as shown in Fig. 2 [9], [10], where R_L and X_i represent the loss resistance and high-frequency reactance, respectively. The matrix can be decomposed into two Z matrices in series, one of which takes account of the contribution of the static coupling and the other of radiative coupling.

A. Static Coupling

The Z matrix for static coupling can be modeled as a simple transformer, which consists of two inductors, L_A^{Tx} and L_A^{Rx} , with a mutual inductance of $M^{Tx,Rx}$:

$$[Z_{\text{stat}}] = \begin{bmatrix} j\omega L_A^{Tx} & j\omega L_M^{Tx,Rx} \\ j\omega L_M^{Tx,Rx} & j\omega L_A^{Rx} \end{bmatrix}. \tag{1}$$

1

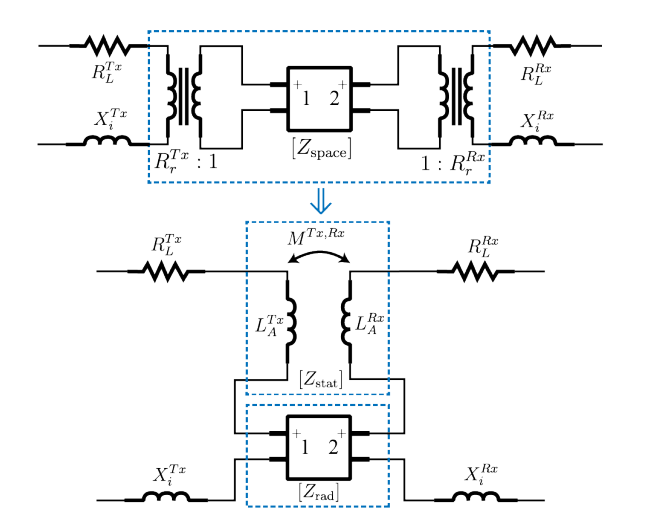


Fig. 2. Circuit model representation of coil coupling within near-field/far-field hybrid region.

It can be proven that the imaginary part of the Poynting vector comes mostly from $1/r_0^2$ and $1/kr_0^3$ terms of magnetic field ${\bf H}$ around a magnetic dipole, and thus the coupling $M^{Tx,Rx}$ can be calculated with the corresponding magnetic flux:

$$M^{Tx,Rx} = \frac{\mu_0 \mathbf{H}_{1/r_0^2, 1/kr_0^3}^{Rx} \cdot \mathbf{S}^{Rx}}{I_0^{Tx}}$$

$$= \frac{\mu_0 S^{Tx} S^{Rx}}{8\pi r_0^2} [3\sin 2\theta_0 \sin \theta_1 \cos \phi_1 + \cos \theta_1 (1 + 3\cos 2\theta_0)] (1 + jkr_0) e^{-jkr_0}, \quad (2)$$

B. Radiative Coupling

The total coupling between two coils can be calculated with the spherical mode coupling method [10]. Here the Z matrix consists of three parts: two transformers representing matching between the Tx/Rx coils and free space, and a $[Z_{\text{space}}]$ matrix that representing mode coupling coefficient. In supplementary material, we calculate the cascaded Z matrix to be:

$$Z_{11/22, {\rm tot}} = R_L^{Tx/Rx} + R_r^{Tx/Rx} + j\omega L_A^{Tx/Rx} + jX_i^{Tx/Rx}, \eqno(3)$$

$$Z_{12,\text{tot}} = Z_{21,\text{tot}} = \sqrt{R_r^{Tx} R_r^{Rx}} A'.$$
 (4)

We estimate the coupling term A' with only the TE_{10} mode, as the coil works as a magnetic dipole:

$$A' = e^{-jkr_0} \left\{ \frac{3}{2} \cos \theta_1 \left[-\sin^2 \theta_0 \frac{1}{jkr_0} + (3\cos^2 \theta_0 - 1) \left(\frac{1}{(jkr_0)^2} + \frac{1}{(jkr_0)^3} \right) \right] + \frac{3}{4} \sin \theta_1 \cos \phi_1 \sin 2\theta_0 \left[\frac{1}{jkr_0} + 3 \left(\frac{1}{(jkr_0)^2} + \frac{1}{(jkr_0)^3} \right) \right] \right\},$$

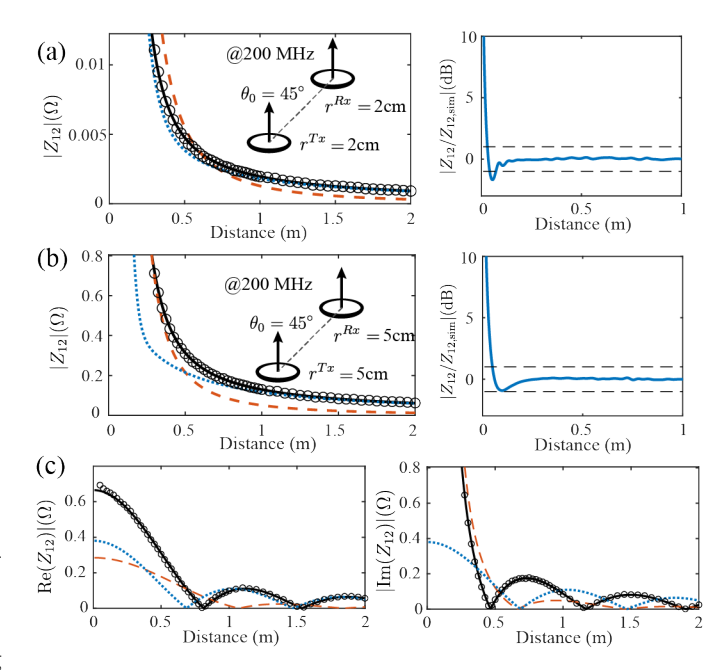


Fig. 3. Calculated coupling term Z_{12} (black solid line) in comparison with simulation results (black dots) for two different coil sizes under the same arrangement. The red and blue dash lines are static and radiative components, respectively. (a) and (b): Same coil placement with different coil diameters. (c) Real/Imaginary part of Z_{12} for setup in (b).

which leaves the radiation terms as:

$$Z_{11/22,\text{rad}} = R_r^{Tx/Rx},$$
 (6)

$$Z_{12,\text{rad}} = Z_{21,\text{tot}} = \sqrt{R_r^{Tx} R_r^{Rx}} A' - j\omega L_M^{Tx,Rx}.$$
 (7)

The radiation resistance R_r can be estimated analytically [11], [12] but can be more easily obtained by simulating or measuring a stand-alone coil.

III. RESULTS AND DISCUSSION

In Fig. 3, we apply the above model to calculate the coupling between coils of two different sizes and compare them with the simulation results with ANSYS HFSS. The results show that the model yields accurate results for a separation larger than 4r. From Fig. 3 (c), one will notice that for a shorter range, the coupling impedance is mostly imaginary due to the direct static coupling between coils, while at a longer distance, the real part emerges, indicating the energy is radiating.

Now we can examine the mechanism of coil coupling with different sizes and placements. As a baseline study, in Fig. 4 we show the static and radiative coupling for coils with various electrical sizes and the boundary that separates the domination of each, which can be considered as a near-field/far-field boundary in many contexts. Different from the general formulas like $d_F=2D^2/\lambda$ or $\lambda/2\pi$, the results show that coils with larger electrical sizes may lead to a closer boundary since more energy is able to couple into space to form a real Poynting vector. Additionally, in Fig. 5, we examine this boundary for the same set of coils with different orientations: although the geometry of the Tx and Rx

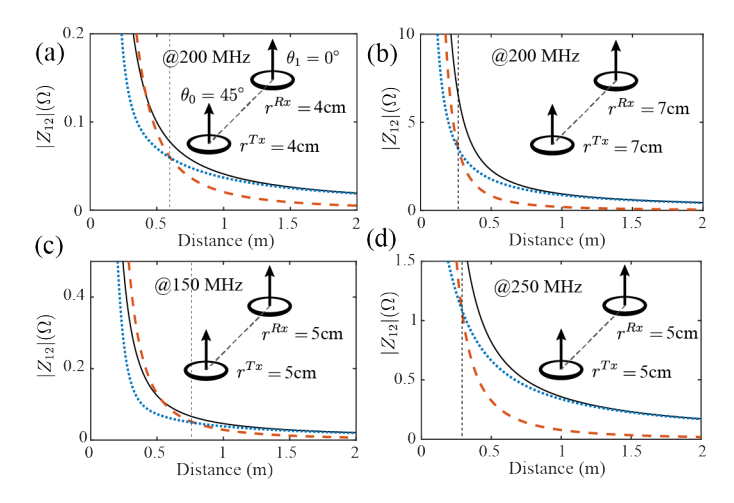


Fig. 4. Z_{12} for four different cases with the same coil placement $\theta_0 = 45^{\circ}$, $\theta_1 = 0$ but different electrical sizes, red and blue dash lines representing static and radiative components, respectively.

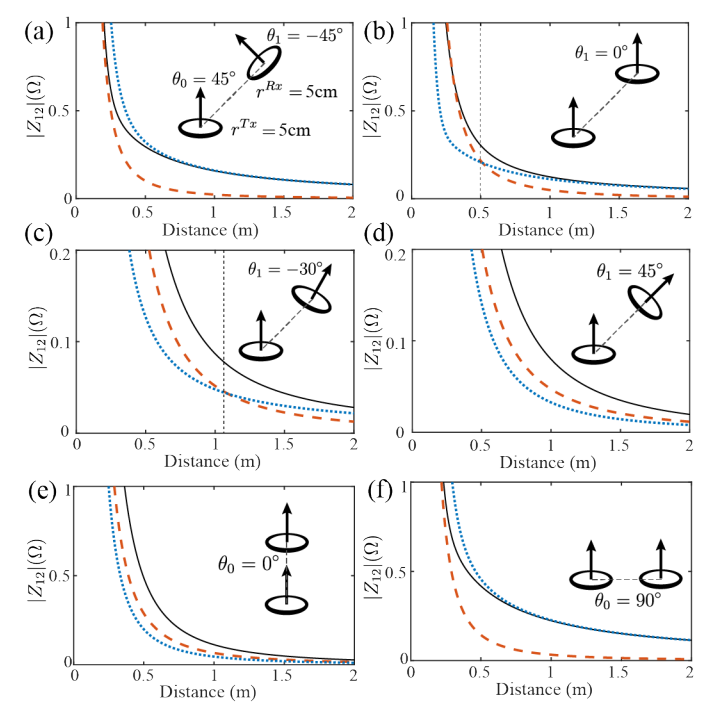


Fig. 5. Z_{12} for six different cases with the same antennas at 200 MHz but different orientations, red and blue dash lines representing static and radiative components, respectively.

remains the same, this cross-point position varies. Therefore, it is not rigorous in any case to give a simple near-field/far-field boundary by merely inspecting the antennas without considering the arrangement of the whole system.

A. Efficiency Consideration

A common objective of using near-field communication to replace far-field radio is to reduce channel loss. Consider two ideal coils working at such a low frequency that only $\left[Z_{\text{stat}}\right]$ is presented, commonly referred to as "quasi-static", one may argue that since no energy radiates to space, the channel efficiency can be maximized. The pitfall of this statement is

that when the static coupling term, i.e. the mutual inductance, is low, even a small resistance R_L may lead to an extremely large dissipation. To demonstrate this, we may examine the maximum available gain (MAG) of a system with [13]:

$$\eta = G_{\text{max}} = |Z_{21}|^2 / q + \sqrt{q^2 - |Z_{12}Z_{21}|^2},$$
(8)

where $q = 2R_r^{Tx}R_r^{Rx} - \text{Re}(Z_{12}Z_{21})$.

In Fig.6, we evaluate this maximum efficiency of the channel of various cases. It can be seen that for $R_L=0$, the efficiency indeed approaches 1 at lower frequencies, but once a small loss is introduced, the efficiency drops drastically. For coils with relatively large apertures and communicating within a short range, an optimal frequency can be found depending on the antenna orientation and loss resistance: generally, a higher loss, a smaller aperture, or a lower static coupling component lead to a high optimal frequency, according to Fig.6(a)(b)(c)(d). When the coil sizes further shrink, or the distance further increases as in Fig.6(e)(f), far-field communication can be the most efficient option for any feasible loss resistance.

B. Bandwidth Consideration

An ideal transformer has an infinitely wide bandwidth, as the input impedance is only dependent on the load side and is independent of frequency. Similarly, the bandwidth of coils that work in the hybrid region also benefits from the static terms. To show this, we first bilaterally match the source and load impedance to obtain a maximum gain at one single frequency f_c :

$$Z_{S/L} = R_{S/L} + jX_{S/L} = \frac{\sqrt{q^2 - |Z_{12}Z_{21}|^2}}{2\text{Re}(Z_{22/11})} + j\left[\text{Im}(Z_{12}Z_{21})/\text{Re}(Z_{22/11}) - \text{Im}(Z_{11/22})\right]$$
(9)

For a frequency band, the input and output impedance are thus:

$$Z_{\text{in/out}} = Z_{11/22} - \frac{Z_{12}Z_{21}}{Z_{22/11} + Z_{L/S}|_{f=f_c}}.$$
 (10)

The reflection on both Tx and Rx sides can then be calculated with the following:

$$\Gamma(f) = \frac{R_S|_{f=f_c} - Z'_{\text{in}}(f)}{R_S|_{f=f_c} + Z'_{\text{in}}(f)}$$
(11)

where $Z'_{in}(f) = Z_{in}(f) + jX_S|_{f=f_c}$.

In Fig. 7, we observe that the bandwidth is effectively broadened when the coils are put closer with a vertical arrangement to increase the static coupling term.

IV. CONCLUSION

An impedance matrix model is developed to quantitatively examine the mechanism of two coils working in the nearfield/far-field hybrid region and we find:

 The position of the "near-field/far-field boundary" depends largely on the configuration of the system as well as the form factor of the coils;

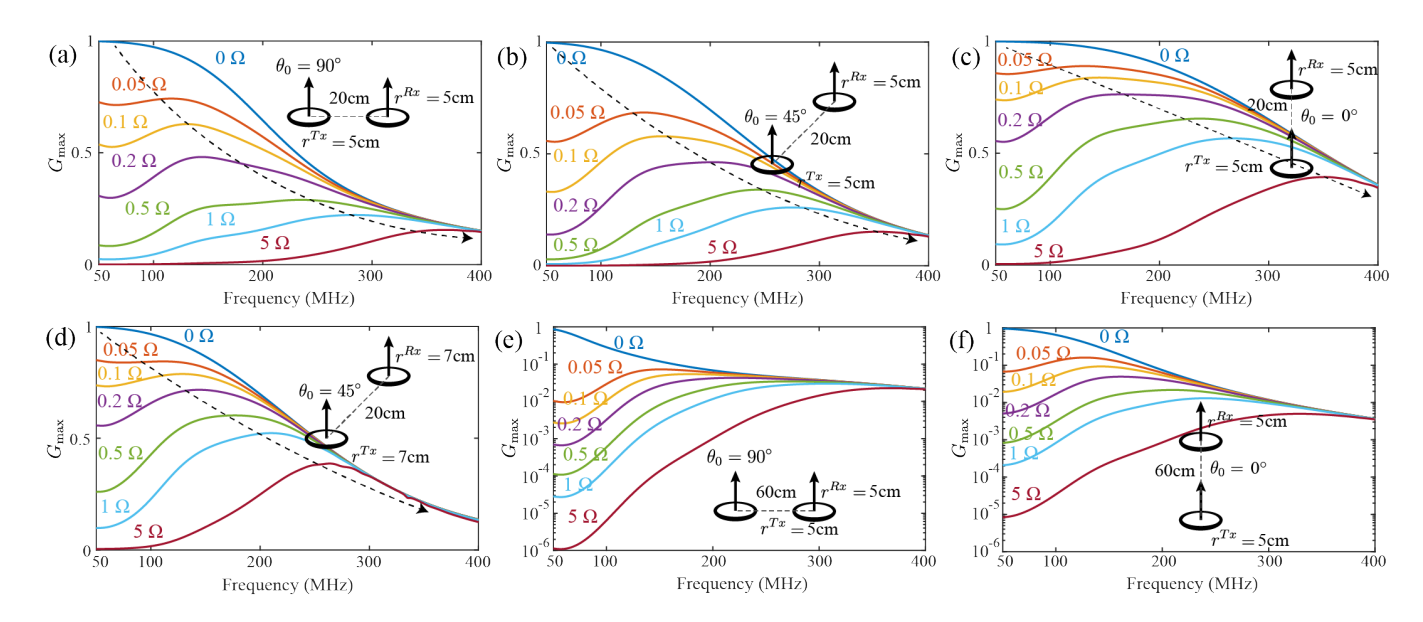


Fig. 6. MAG of the channels using various setups under different R_L . The dashed lines with arrows indicate the trends of optimal frequency change with respect to increasing loss.

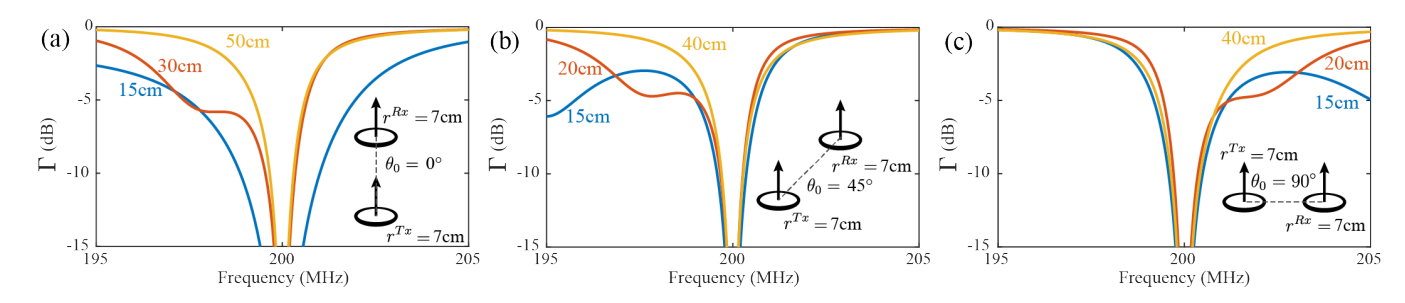


Fig. 7. Reflection coefficient at the Tx/Rx input ports of two coils matched bilaterally at 200 MHz.

- channel efficiency in the hybrid region is sensitive to losses. For large antennas operating over a short range, one may find an optimal frequency to minimize the channel loss, and
- 3) one can take advantage of the static field coupling component to increase the bandwidth of the channel.

It is also worth mentioning that other forms of near-field communication, such as capacitive coupling, can be analyzed in a similar manner by replacing eq. (5) with TM modes and eq. (2) with a capacitive coupling term. As more near-field communication systems emerge, we believe this model gives an insight into how those channels work. More importantly, especially for high-frequency channels, the mechanism should always be verified with a similar model as in this letter when making modeling assumptions.

REFERENCES

- Z. Zhang, H. L. Pang, A. Georgiadis, and C. Cecati, "Wireless Power Transfer-An Overview," *IEEE T Ind Electron*, vol. 66, no. 2, pp. 1044-1058, Feb 2019.
- [2] S. Maity, M. X. He, M. Nath, D. Das, B. Chatterjee, and S. Sen, "Bio-Physical Modeling, Characterization, and Optimization of Electro-Quasistatic Human Body Communication," *IEEE T Bio-Med Eng*, vol. 66, no. 6, pp. 1791-1802, Jun 2019.
- [3] E. D. Wen, D. F. Sievenpiper, and P. P. Mercier, "Channel Characterization of Magnetic Human Body Communication," *IEEE T Bio-Med Eng*, vol. 69, no. 2, pp. 569-579, Feb 2022.

- [4] H. J. Kim, H. Hirayama, S. Kim, K. J. Han, R. Zhang, and J. W. Choi, "Review of Near-Field Wireless Power and Communication for Biomedical Applications," *IEEE Access*, vol. 5, pp. 21264-21285, 2017.
- [5] S. R. Khan, S. K. Pavuluri, and M. P. Y. Desmulliez, "Accurate Modeling of Coil Inductance for Near-Field Wireless Power Transfer," *IEEE T Microw Theory*, vol. 66, no. 9, pp. 4158-4169, Sep 2018.
- [6] P. P. Mercier and A. P. Chandrakasan, "Rapid Wireless Capacitor Charging Using a Multi-Tapped Inductively-Coupled Secondary Coil," *IEEE T Circuits-I*, vol. 60, no. 9, pp. 2263-2272, Sep 2013.
- [7] P. P. Mercier and A. P. Chandrakasan, *Ultra-low-power Short-range Radios*. Springer, 2015.
- [8] J. Park, H. Garudadri, and P. P. Mercier, "Channel Modeling of Miniaturized Battery-Powered Capacitive Human Body Communication Systems," *IEEE T Bio-Med Eng*, vol. 64, no. 2, pp. 452-462, Feb 2017.
- [9] A. C. Gately, D. J. R. Stock, and B. R. S. Cheo, "A Network Description for Antenna Problems," *Pr Inst Electr Elect*, vol. 56, no. 7, pp. 1181-1193,1968.
- [10] J. Lee and S. Nam, "Fundamental Aspects of Near-Field Coupling Small Antennas for Wireless Power Transfer," *IEEE Transactions on Antennas and Propagation*, vol. 58, no. 11, pp. 3442-3449, Nov 2010.
- [11] J. E. Storer, "Impedance of thin-wire loop antennas," *Transactions of the American Institute of Electrical Engineers, Part I: Communication and Electronics*, vol. 75, no. 5, pp. 606-619, 1956.
- [12] C. A. Balanis, Antenna theory: analysis and design. John wiley & sons, 2015.
- [13] D. M. Pozar, Microwave engineering. John wiley & sons, 2011.